Dalton Transactions

ROYAL SOCIETY OF CHEMISTRY

PAPER

View Article Online
View Journal | View Issue

Cite this: *Dalton Trans.*, 2025, **54**, 12503

The miracle of self-assembly: a journey of the $\{Ln_6F_8\}$ core in the world of lanthanides

Evgeny D. Boltkov, *[a] Mikhail E. Buzoverov,[b] Elmira Kh. Lermontova,[b] Yury A. Belousov, [a,d] Dmitry A. Steshenko,[a] Victoria E. Gontcharenko[c,d] and Tatyana Yu. Glazunova[a]

This work presents a unique example of the self-assembly of $\{Ln_6F_8\}$ clusters composed of Ln^{3+} cations and F^- and CF_3COO^- anions. The crystal structures of new fluorotrifluoroacetate compounds with the general formula **$A_2[Ln_6(\mu_3\text{-}F)_8(tfa)_{12}L_6]$**, where A = Na and Ln = Pr(I), Eu (**IIa**), Tb(III), Dy(IV) and Tm(V); A = Na and H_3O^+ and Ln = Eu (**IIb**); or A = K and Ln = Yb(VI); tfa = CF_3COO^- (trifluoroacetate anion); L = Htfa (CF_3COOH, trifluoroacetic acid) and H_2O, determined by the single-crystal XRD method revealed that they were constructed from the complex anion **$[Ln_6(\mu_3\text{-}F)_8(tfa)_{12}L_6]^{2-}$** and alkali metal (or alkali metal and hydroxonium) cations and included solvate molecules in some cases. The core of the anion presented a rhombododecahedral unit of six lanthanide atoms linked by bridging fluoride and trifluoroacetate anions. The nature of the counterion led to the formation of compounds with different dimensions: from 1D for potassium cations and 2D for sodium cations to 3D for sodium and hydroxonium cations. The $\{Ln_6F_8\}$ clusters were obtained for a wide range of lanthanides, with Pr and Yb being the end members; thus, the existence of heterometallic compounds was presumed. At a temperature of 100 °C, the new compounds started to release solvent molecules, whereas the **$[Ln_6(\mu_3\text{-}F)_8(tfa)_{12}]$** core was stable up to 270–300 °C according to the TG-MS data. Substances **IIb**, **III** and **IV** revealed metal-centered luminescence and could be used for the development of new optoelectronic materials.

Received 10th May 2025,
Accepted 20th July 2025

DOI: 10.1039/d5dt01105a

rsc.li/dalton

1. Introduction

Lanthanide carboxylates find a lot of applications due to their luminescence properties, allowing the production of luminescent materials and chemical sensors based on them.[1–3] The possibility of using carboxylic acids with a specific structure and additional functional groups, as well as the high coordination numbers of lanthanides, determines the wide variety of representatives of this group of compounds.

Our research group has been intensively interested in fluorocarboxylates of various transition metals.[4,5] The addition of fluoride ions to the system allows the assembly of small clusters stabilized by carboxylate anions. In this case, only the stoichiometry of the reagents determines the nuclearity and structure of the cluster as opposed to oxo- or hydroxo-clusters, for which hydrolysis processes play an important role, and as a consequence, the acidity of the reaction mixture and the amount of water also require control.

A literature review showed that most characterized lanthanide fluorocarboxylate compounds contain the $\{Ln_6(\mu_3\text{-}F)_8\}$ core.[6–10] The first work studying such compounds was published in 2020.[9] A compound $[Tb_6(\mu_3\text{-}F)_8(piv)_{10}(Hpiv)_4DMF]\cdot x DMF\cdot y H_2O$ (Hpiv = pivalic acid, DMF = dimethylformamide) was characterized by SCXRD, and researchers were able to describe its structure. The molecular fragment $[Tb_6(\mu_3\text{-}F)_8(piv)_{10}(Hpiv)_4DMF]$ was based on an octahedron of six terbium atoms. Eight fluorine atoms were placed over each $\{Ln_3\}$ face of the octahedron, and ten pivolate anions connected the terbium atom pairs. DMF and Hpiv molecules completed the coordination environment of the terbium atoms. The presence of F^- ions was confirmed by XPS and MALDI-TOF methods. A study on the photophysical properties of $[Tb_6(\mu_3\text{-}F)_8(piv)_{10}(Hpiv)_4DMF]\cdot x DMF\cdot y H_2O$ revealed its extremely high quantum yield (99.6%) and luminescent lifetime (2.03 ms). These characteristics were better than those for similar hydroxoclusters and nanoscale TbF_3. Analyzing the data, the authors conclude that the central $\{Tb_6(\mu_3\text{-}F)_8\}$ core

[a]*M.V. Lomonosov Moscow State University, Department of Chemistry, Moscow 119991, Russia. E-mail: boltkov@inorg.chem.msu.ru*
[b]*N.S. Kurnakov General and Inorganic Chemistry Institute, Russian Academy of Sciences, Leninskii Pr. 31, Moscow 119991, Russia*
[c]*Faculty of Chemistry, National Research University Higher School of Economics, 20 Miasnitskaya Str., Moscow 101000, Russia*
[d]*P. N. Lebedev Physical Institute of the Russian Academy of Sciences, 53 Leninskiy 1. Prospect, Moscow, 119991, Russia*

acts as an energy cage that minimizes the energy loss caused both by energy migration and multiphonon relaxation. Thus, the presented work described lanthanide fluorocarboxylates as promising substances that could be used to produce luminescent materials.

Independently, Morsbach *et al.*[6,10] serendipitously obtained complexes $[(NH_4)_{0.75}(H_3O)_{0.25}]_2[Yb_6(\mu_3\text{-}F)_8(tfa)_{12}(H_2O)_4]\cdot 4H_2O$,[6] $(NH_4)_2[Eu_6(\mu_3\text{-}F)_8(tfa)_{12}(Htfa)_6]$ and $(NH_4)_2[Eu_6(\mu_3\text{-}F)_8(pfa)_{12}(Hpfa)_6]\cdot 8Hpfa$[10] (Hpfa = pentafluoropropionic acid) during attempts to synthesize the simple perfluorocarboxylates of Eu^{2+} and Yb^{2+} in liquid ammonia. The europium hexanuclear side-products exhibited longer luminescence decay times than related μ_3-OH-capped compounds. Notably, the synthetic mixtures did not contain any fluoride sources, but the $\{Ln_6(\mu_3\text{-}F)_8\}$ cores were assembled through slow oxidation processes. The possible cause of cluster formation may be activation of C–F bonds by binding of a fluoride atom to a lanthanide ion at an intermediate stage, as suggested by Vizuet *et al.*[7] In that work, the question of the composition of the UiO-66 type lanthanide MOF (containing $\{Ln_6(\mu_3\text{-}OH)_8\}$ cores) formed in the presence of a fluorine modulator was addressed for the first time. The reexamination was supported by SCXRD, XPS, IR, SEM/EDS and NMR experimental data and showed that the presence of a fluoride atom in the μ_3 positions is more consistent with this data. Thus, the number of known compounds based on $\{Ln_6(\mu_3\text{-}F)_8\}$ clusters could be significantly higher due to the inclusion of metal organic frameworks synthesized in the presence of 2-fluorobenzoic acid (2-fba) or 2,6-difluorobenzoic acid (2,6-fba) as modulators. Additionally, when the authors[7] examined the use of an extra amount of modulator under the same conditions, leading to the formation of HoF_3, the results also confirmed the C–F bond activation. To sum up, in terms of their photoluminescent properties, compounds containing the $\{Ln_6(\mu_3\text{-}F)_8\}$ unit are more promising than their μ_3-OH analogues, and their synthesis is relatively straightforward. Given that these compounds have not yet been studied in depth, there is significant motivation for work in this area.

Herein, we report the synthesis under mild conditions of a series of new isotype fluorotrifluoroacetate hexanuclear complexes of Pr(III), Eu(III), Tb(III), Dy(III), Tm(III) and Yb(III), with the general anion fragment $[\mathbf{Ln_6(\mu_3\text{-}F_8)(tfa)_{12}L_6}]^{2-}$, containing a unique $\{Ln_6(\mu_3\text{-}F)_8\}$ core. Trifluoroacetate anions were chosen due to the absence of X–H bonds capable of acting as vibrational quenchers. The optimized conditions allowed large crystals of seven compounds containing alkali metal (Na and K) counterions to be obtained: $Na_2[\mathbf{Pr_6(\mu_3\text{-}F_8)(tfa)_{12}}(Htfa)_2(H_2O)_4](Htfa)_{0.5}$ (**I**), $Na_2[\mathbf{Eu_6(\mu_3\text{-}F_8)(tfa)_{12}}(Htfa)_{0.88}(H_2O)_{5.12}]$ (**IIa**), $(H_7O_3)_{0.5}Na_{1.5}[\mathbf{Eu_6(\mu_3\text{-}F_8)(tfa)_{12}}(Htfa)_{0.78}(H_2O)_{5.22}](Htfa)_{0.72}(H_2O)_{1.5}$ (**IIb**), $Na_2[\mathbf{Tb_6(\mu_3\text{-}F_8)(tfa)_{12}}(Htfa)_{0.88}(H_2O)_{5.12}]$ (**III**), $Na_2[\mathbf{Dy_6(\mu_3\text{-}F_8)(tfa)_{12}}(Htfa)_2(H_2O)_4](Htfa)_{0.5}$ (**IV**), $Na_2[\mathbf{Tm_6(\mu_3\text{-}F_8)(tfa)_{12}}(Htfa)_2(H_2O)_4](Htfa)_{0.5}$ (**V**), and $K_2[\mathbf{Yb_6(\mu_3\text{-}F_8)(tfa)_{12}}(H_2O)_5](Htfa)_2(H_2O)$ (**VI**). The compounds were studied by SCXRD, PXRD, IR, and DSC-TG analyses. Their crystal structure is discussed in comparison with the above-mentioned analogues. The luminescent properties of compounds **IIb**, **III** and **IV** were also studied.

2. Experimental

2.1. Synthesis of I–VI

For the syntheses, the following set of lanthanide precursors was used: $Pr_2(CO_3)_3\cdot 6H_2O$ (reagent grade), $Eu_2(CO_3)_3\cdot 3H_2O$ (reagent grade), $Tb_2(CO_3)_3\cdot 3H_2O$ (reagent grade), $Dy_2(CO_3)_3\cdot 4H_2O$ (reagent grade), $Tm_2(CO_3)_3\cdot 4H_2O$ (reagent grade), and $Yb_2(CO_3)_3\cdot 3H_2O$ (reagent grade) along with fluorides NaF (high-purity grade), KHF_2 (high-purity grade), acids HF (48%, high-purity grade), and Htfa (99%, high-purity grade) and phosphorus pentoxide P_4O_{10} (reagent grade). Alkali metal fluorides were added to the reaction mixture as a 0.125 M water solution, HF was added as a 0.375 M water solution.

The synthesis was performed using the same procedure for all compounds. The hexahydrate of the lanthanide carbonate (Ln = Pr, Eu, Tb, Dy, Tm or Yb) was dissolved in 90% trifluoroacetic acid at room temperature, then a mixed solution of alkali metal fluoride and hydrofluoric acid was added. The molar ratio of the ions M^+ (M = Na and K), Ln^{3+} and F^- in the reagent was 1 : 3 : 4 (Table S1).

The solutions obtained were placed in a desiccator containing phosphorus pentoxide at room temperature, leading to the formation of bulk crystals with linear lengths up to 0.3 cm, which were suitable for SCXRD. The reaction mixture for the europium sample gave two types of crystals with different shapes (**IIa** and **IIb**) that could be separated manually. After two weeks, the formed crystals were removed from the mother liquor and dried in an argon flow. Compounds **I–VI** were stable in air for long times.

2.1.1 $Na_2[Pr_6(\mu_3\text{-}F_8)(tfa)_{12}(Htfa)_2(H_2O)_4](Htfa)_{0.5}$ (I). Obtained from 0.620 g (2.177 mmol) $Pr_2(CO_3)_3\cdot 6H_2O$, 2.91 mL NaF/HF solution (0.726 mmol NaF and 2.902 mmol HF). Yield: 62%. IR: 3200–3700, 1768, 1699, 1631, 1607, 1468, 1450, 1215, 1152, 848, 801, 727, 706, 612, 522, 467, 441. Content of Pr: calculated 30.7%, found 30.3%.

2.1.2 $Na_2[Eu_6(\mu_3\text{-}F_8)(tfa)_{12}(Htfa)_{0.88}(H_2O)_{5.12}]$ (IIa) and $(H_7O_3)_{0.5}Na_{1.5}[Eu_6(\mu3\text{-}F8)(tfa)_{12}(Htfa)_{0.78}(H_2O)_{5.22}](Htfa)_{0.72}(H_2O)_{1.5}$ (IIb). Obtained from 0.607 g (2.257 mmol) $Eu_2(CO_3)_3\cdot 3H_2O$, 3.01 mL NaF/HF solution (0.752 mmol NaF and 3.009 mmol HF). **IIa** IR: 3200–3700, 1771, 1710, 1702, 1612, 1471, 1215, 1157, 850, 800, 728, 616, 522, 471, 447. Content of Eu: calculated 34.3%, found 34.5%. **IIb** IR: 3200–3700, 1767, 1702, 1619, 1474, 1215, 1157, 851, 802, 728, 615, 522, 470, 446. Content of Eu: calculated 32.9%, found 33.1%.

2.1.3 $Na_2[Tb_6(\mu_3\text{-}F_8)(tfa)_{12}(Htfa)_{0.88}(H_2O)_{5.12}]$ (III). Obtained from 0.633 g (2.222 mmol) $Tb_2(CO_3)_3\cdot 3H_2O$, 2.96 mL NaF/HF solution (0.741 mmol NaF and 2.963 mmol HF). Yield: 59%. IR: 3200–3700, 1773, 1716, 1703, 1628, 1610, 1475, 1216, 1157, 852, 802, 728, 703, 617, 522, 473, 449. Content of Tb: calculated 35.3%, found 35.6%.

2.1.4 $Na_2[Dy_6(\mu_3\text{-}F_8)(tfa)_{12}(Htfa)_2(H_2O)_4](Htfa)_{0.5}$ (IV). Obtained from 0.603 g (2.079 mmol) $Dy_2(CO_3)_3\cdot 4H_2O$, 2.78 mL NaF/HF solution (0.693 mmol NaF and 2.772 mmol HF). Yield: 63%. IR: 3200–3700, 1780, 1714, 1702, 1627, 1608, 1476, 1457, 1215, 1155, 853, 802, 729, 703, 618, 523, 473, 450. Content of Dy: calculated 33.8%, found 33.5%.

2.1.5 $Na_2[Tm_6(\mu_3\text{-}F_8)(tfa)_{12}(Htfa)_2(H_2O)_4](Htfa)_{0.5}$ (V). Obtained from 0.608 g (2.051 mmol) $Tm_2(CO_3)_3{\cdot}4H_2O$, 2.74 mL NaF/HF solution (0.684 mmol NaF and 2.735 mmol HF). Yield: 61%. IR: 3200–3700, 1783, 1719, 1706, 1628, 1610, 1477, 1217, 1158, 854, 801, 729, 701, 619, 523, 476, 454. Content of Tm: calculated 34.7%, found 34.8%.

2.1.6 $K_2[Yb_6(\mu_3\text{-}F_8)(tfa)_{12}(H_2O)_5](Htfa)_2(H_2O)$ (VI). Obtained from 0.588 g (2.027 mmol) $Yb_2(CO_3)_3{\cdot}3H_2O$, 2.71 mL KF/HF solution (0.676 mmol KF and 2.702 mmol HF). Yield: 67%. IR: 3200–3700, 1705, 1612, 1478, 1215, 1155, 854, 801, 729, 701, 618, 522, 480, 458. Content of Yb: calculated 35.1%, found 35.0%.

2.2. Methods and equipment

All studies, excluding PXRD and SCXRD experiments, were performed with the same large single crystals of compounds after confirmation of their composition and structure by SCXRD analysis of splinters of each crystal.

PXRD data were collected using a Huber G670 Guinier Camera ($CuK_{\alpha1}$ radiation, Ge monochromator, λ = 1.5406 Å). Le Bail refinement was performed using Jana2020 software.[11]

Single crystals of compounds **I–VI** were subjected to X-ray single-crystal measurements with a Bruker diffractometer (AXS D8 VENTURE PHOTON III C14 IuS 3.0 and SMART-APEX-II) using graphite monochromatized MoK_α radiation under a stream of cooled nitrogen. Data reduction was performed using the SAINT program.[12] Absorption correction based on measurements of equivalent reflections was applied.[13] Structures were solved by direct methods and refined by F^2 by full-matrix least-squares in anisotropic approximation for non-hydrogen atoms using the SHELXTL-Plus software.[14] For all structures, hydrogen atoms were placed in the calculated positions. In all the structures, the $-CF_3$ groups are rotationally disordered and were refined with restrained C–F and F···F distances (SADI). In the structures of monoclinic compounds **IIa** and **III**, there is statistical disordering of the axial ligands. The occupancies of the H_2O (PART 1) and Htfa (PART 2) molecules were refined using a free variable (oc(H_2O) + oc(Htfa) = 1) and then fixed. The Htfa molecule was refined isotropically with restriction of the C–F, C–C and F···F distances (DFIX commands). The ADP of these fluorine atoms were unified using the EADP command. The same disordering was observed in **IIb**, but one more Htfa solvate molecule was observed in the H_2O PART connected to water *via* a hydrogen bond. All the restrictions applied to the Htfa molecules were identical to those described above, and the disordered molecules were refined isotropically. Moreover, there were voids in this net-like structure, filled by H_3O^+ cations and H_2O molecules. Because of the poor sensitivity of the SCXRD method to hydrogen atoms and their complex disordering, only oxygen atoms (five different PART positions) in the voids were added to the model. Potassium complex **VI** has another type of disordering. One of the bridging trifluoroacetate anions either occupies the standard position between two Yb atoms (major PART) or connects the Yb and K atoms (minor PART). Both PARTs were supplemented by water molecules on the atom that did not bind with trifluoroacetate anions (K and Yb atom in the major and minor PART, respectively). The occupancies of the PARTs were refined using a free variable and then fixed. The minor PART was refined isotropically. The Htfa molecule was refined isotropically with restriction of the C–F (DFIX commands), C–C and F···F distances (SADI commands). The ADP of these fluorine atoms were unified using the EADP command.

A summary of the crystallographic data and structure determination parameters is provided in Table S2. Crystal data have been deposited in the Crystallographic Data Centre as supplementary publications under the CCDC numbers 2391137–2391142 and 2427723.

Infrared spectra were recorded with an FTIR Spectrum One (PerkinElmer). The samples were pressed into KBr pellets and measured. The spectral resolution was 0.5 cm^{-1}, from 4000 cm^{-1} to 400 cm^{-1}.

The TG-DSC thermal analysis of samples combined with a simultaneous QMS evolved gas analysis was performed in a dynamic stream of argon (30 mL min^{-1}) with an STA 409PC/PG (NETZSCH) at 25 °C to 500 °C with a 5 K min^{-1} heating rate.

Photoluminescence and excitation spectra in the visible region for all the complexes were measured in the solid state using a Horiba Jobin–Yvon Fluorolog QM-75-22-C spectrofluorimeter fitted with a 75 W xenon arc lamp (ArcTune). A Hamamatsu R13456 cooled photomultiplier tube that was sensitive in the UV-Vis-NIR region (200–950 nm) was used as the detector. Photoluminescent decays were recorded for all the complexes in the solid state using the same device, except the excitation source was changed to a pulsed xenon lamp with a 50 μs pulse duration and 100 Hz repetition rate.

3. Results and discussion

In the present work, we report seven new fluorotrifluoroacetate complexes of lanthanides (structures were determined from single-crystal XRD experiment data):

$Na_2[Pr_6(\mu_3\text{-}F_8)(tfa)_{12}(Htfa)_2(H_2O)_4](Htfa)_{0.5}$ (**I**)

$Na_2[Eu_6(\mu_3\text{-}F_8)(tfa)_{12}(Htfa)_{0.88}(H_2O)_{5.12}]$ (**IIa**)

$(H_7O_3)_{0.5}Na_{1.5}[Eu_6(\mu_3\text{-}F_8)(tfa)_{12}(Htfa)_{0.78}(H_2O)_{5.22}](Htfa)_{0.72}(H_2O)_{1.5}$ (**IIb**)

$Na_2[Tb_6(\mu_3\text{-}F_8)(tfa)_{12}(Htfa)_{0.88}(H_2O)_{5.12}]$ (**III**)

$Na_2[Dy_6(\mu_3\text{-}F_8)(tfa)_{12}(Htfa)_2(H_2O)_4](Htfa)_{0.5}$ (**IV**)

$Na_2[Tm_6(\mu_3\text{-}F_8)(tfa)_{12}(Htfa)_2(H_2O)_4](Htfa)_{0.5}$ (**V**)

$K_2[Yb_6(\mu_3\text{-}F_8)(tfa)_{12}(H_2O)_5](Htfa)_2(H_2O)$ (**VI**)

The synthetic method used was simple and allowed to obtain large crystals of these compounds (Fig. 1). Both big crystal sizes and stability at ambient atmosphere made it possible to study the samples by IR-spectroscopy, TG-MS and luminescence measurements using parts of one single crystal. Nevertheless, phase purity of the obtained solid products was explored by the PXRD method (Fig. S1–S7, and Table S3), which was needed to characterize the synthetic procedure.

Crystalline compounds formed in solutions during the concentration process were not produced as single-phase samples in some cases. Phase analysis of the europium system shows

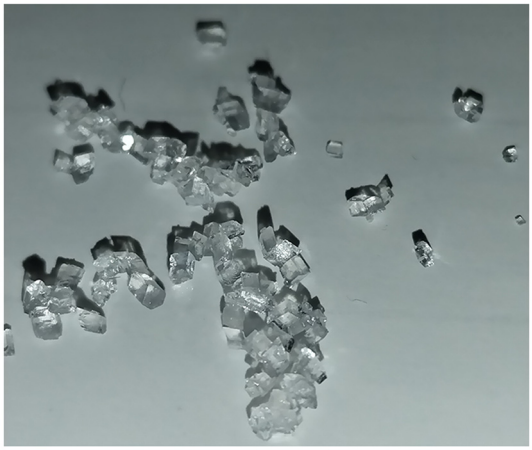

Fig. 1 Photograph of the as-synthesized compound **IIb**.

the presence of two compounds with slightly different compositions and structures (the crystals could be separated manually based on their morphology). It was also found that the solid substance formed in the synthesis of **I** contained small amounts of impurities. We repeated the synthesis of Pr compound **I** several times and found that the resulting solids contained the same impurity. However, the single notable peak did not allow us to conduct a phase analysis to establish its nature; thus, some of these systems require further studies.

IR spectra of **I–VI** show the presence of absorption bands corresponding to vibrations of atom groups in trifluoroacetate anions, trifluoroacetic acid and water (Fig. S8, and Table S4). Band assignments were made based on data from published articles[15–17] in which the IR spectra of trifluoroacetates were also discussed. No bands corresponding to ν(Ln–O) oscillations were observed in the studied region; these probably absorb slightly more to the right than 400 cm^{-1}. However, a shift of the absorption band corresponding to the planar vibration of the CCOO-group (that is directly related to the energy of the Ln–O bonds) was observed. The reduction of the lanthanide ionic radius in the series of compounds **I–VI** leads to increasing Ln–O bond energy and, correspondingly, to a shift in the $\delta_{oop}(CCO_2)$ band to the higher wavenumbers.

Despite the diversity of the lanthanide carboxylates and their tendency to form oligo- and poly-nuclear coordination compounds, to our knowledge, there are only five reports of compounds featuring a $\{Ln_6F_8\}$ core.[6,7,9,10,18] A pivalate complex $[Tb_6(\mu_3\text{-}F)_8(piv)_{10}(Hpiv)_4DMF]\cdot xDMF\cdot yH_2O$ was the first reported compound of this type.[9] Trifluoroacetate and pentafluoropropionate analogies with the same fragment $[Ln_6(\mu_3\text{-}F_8)(tfa)_{12}L_6]^{2-}$ were subsequently described.[10] Meanwhile, the results reported in the present work indicate the existence of a family of compounds structurally related to fluorocarboxylatolanthanate for the wide row of lanthanides (at least from Pr to Yb).

The presence of the second phase **IIb** $((H_7O_3)_{0.5}Na_{1.5}[Eu_6(\mu_3\text{-}F)_8(tfa)_{12}(Htfa)_{0.78}(H_2O)_{5.22}](Htfa)_{0.72}(H_2O)_{1.5})$ in the system Na–Eu–tfa–F additionally indicates the stability of the fluorotrifluoroacetic fragment $[Ln_6(\mu_3\text{-}F)_8(tfa)_{12}L_6]$. We associate the formation of **IIb** with some non-stoichiometry of the europium carbonate hydrate, leading to a lack of sodium ions in the reaction mixture. In this case, the compound contains hydroxonium cations as compensation.

3.1. Structure description

According to SCXRD data, compounds **I–VI** have a unique architecture of the anion complex, which contains the $[Ln_6(\mu_3\text{-}F)_8(tfa)_{12}]$ fragment common for all substances. The fragment is formed by six Ln atoms placed at the vertices of the almost ideal octahedra (Fig. 2). Eight fluorine atoms connect three neighboring lanthanide atoms in positions above the octahedra faces. Each pair of Ln atoms is additionally linked *via* bridging trifluoroacetate anions. The fragment structure is similar to analogs described in the literature.[9,10]

Axial positions (the ninth donor atom positions for Ln^{3+} ions) are occupied by molecules of water or trifluoroacetic acid. In the structures of compounds **IIa**, **IIb**, **III**, and **VI**, these molecules are statistically disordered. The hydrogen atoms of the trifluoroacetic acids in the axial positions form intramolecular hydrogen bonds with oxygen atoms of the bridging trifluoroacetate anions (Fig. 3).

Axial ligands are absent at some lanthanide atoms in compound **VI**, which is based on ytterbium atoms with a smaller radius than the other lanthanides in compounds reported in

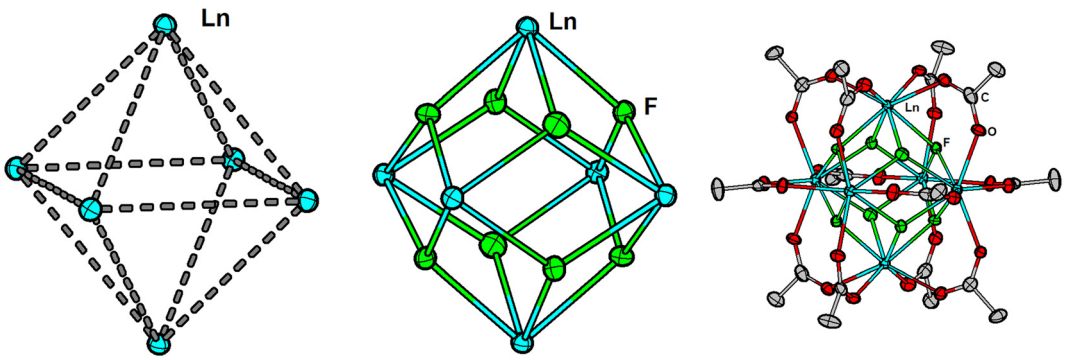

Fig. 2 Structure of the anionic fragment $[Ln_6(\mu_3\text{-}F)_8(tfa)_{12}]$. In the last picture, fluorine atoms of the CF_3-groups are omitted for clarity.

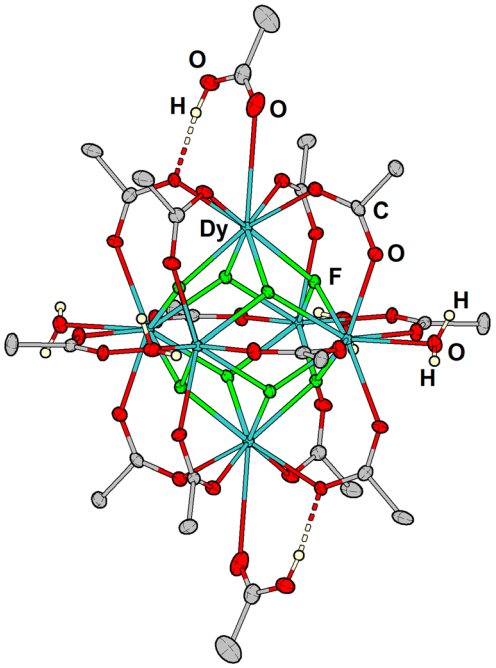

Fig. 3 Fragment of the anion complex in the crystal structure of **IV**. The intramolecular hydrogen bonds are shown in dashed lines, and the fluorine atoms of the CF_3-groups are omitted for clarity.

this work. Consequently, a coordination number of 8 for the Yb ion was observed. The observation was also noted in recently published works[6] on ytterbium fluorotrifluoroacetate complexes with a rhombododecahedral core. Another reason for the lower coordination number could be steric hindrance, as observed for similar pivalate complexes.[9]

Coordination polyhedra of the Ln atoms were determined using the continuous shape measures (CShM) approach implemented in SHAPE2.1 software[19] (Table S6). According to the calculated data, the best description of the polyhedra for lanthanides with CN = 9 is a capped square antiprism (C_{4v}), whereas for the ytterbium atoms in **VI** (CN = 8) without axial ligands, the most accurate description of a polyhedron is a square antiprism (D_{4d}).

Reduction of the lanthanide ionic radii along the Pr–Yb row (structures **I–VI**) causes the shortening of the Ln–Ln, Ln–F, and Ln–O lengths and is consistent with theoretically calculated data[20] (Table 1).

Alkali metal cations (sodium or potassium) play the role of counterions for the described anion complexes. In structures **I–VI**, the cations are located between two neighboring anions and have six oxygen atoms in their environment (Fig. 4). For the larger potassium cation, the environment also includes one additional oxygen atom from a trifluoroacetic acid molecule.

It is worth noting that, in structures **I–V**, a few fluorine atoms of the CF_3 groups are close to the sodium ions. As we highlight above, the reduction of the lanthanide radius leads to the shrinkage of the $\{Ln_6(\mu_3\text{-}F)_8\}$ core. At the same time, the Ln–O distances increase (O atoms are from the trifluoroacetate anion connected to Na ions). This, in turn, makes sodium atoms more available to contact the fluorine atoms of the CF_3 groups, so the Na···F distances become shorter in the series of compounds **I–V** (Fig. 5). Calculations (Fig. S17, Tables S8–S13) by the overlapping spheres method[21] indicate that the coordination number of sodium ions in **I–V** is almost constant (excluding Na1 atom in structure of **I**) and is 10. At the same time, the proportion of the specific surface area of the Voronoi–Dirichlet polyhedra per six oxygen atoms in the

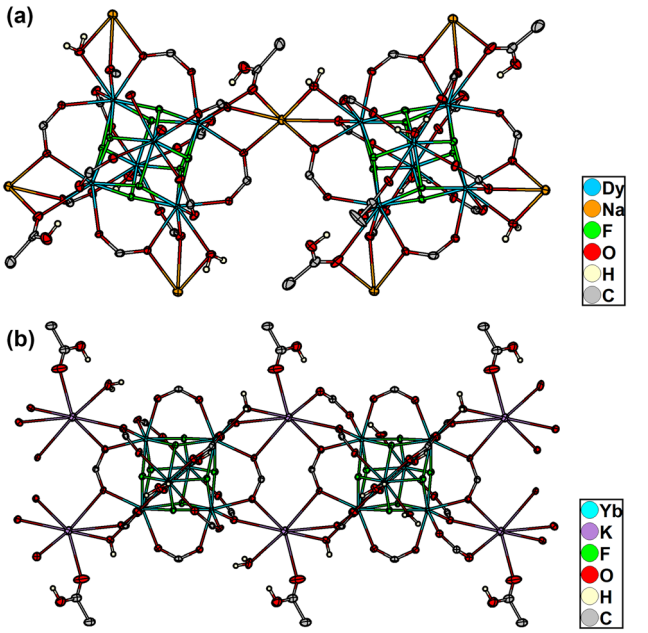

Fig. 4 Environment of the alkali metal ions: (a) sodium in compound **IV** and (b) potassium in compound **VI**. Fluorine atoms of the CF_3-groups are omitted for clarity.

Table 1 Average Ln–F and Ln–O (oxygen atoms from bridging trifluoroacetate anions) bond lengths and Ln–Ln distances for the nine-coordinated Ln ions for compounds **I–VI**

	Pr(I)	Eu (**IIa**)	Eu (**IIb**)	Tb(III)	Dy(IV)	Tm(V)	Yb(VI)
***d*(Ln···Ln)**	**4.0738(5)**	**3.9859(7)**	**3.9804(9)**	**3.9457(8)**	**3.9232(6)**	**3.8617(5)**	**3.8537(4)**
***d*(Ln–F)**	**2.428(3)**	**2.378(4)**	**2.376(4)**	**2.352(6)**	**2.342(3)**	**2.309(3)**	**2.304(2)**
***d*(Ln–O_{tfa})**	**2.474(4)**	**2.405(6)**	**2.400(5)**	**2.375(8)**	**2.359(4)**	**2.318(3)**	**2.307(5)**
d(Ln–F)$_{theor.}$	2.44	2.37	2.37	2.34	2.33	2.29	2.28 (CN 8)
d(Ln–O)$_{theor.}$	2.49	2.42	2.42	2.39	2.38	2.34	2.33 (CN 8)

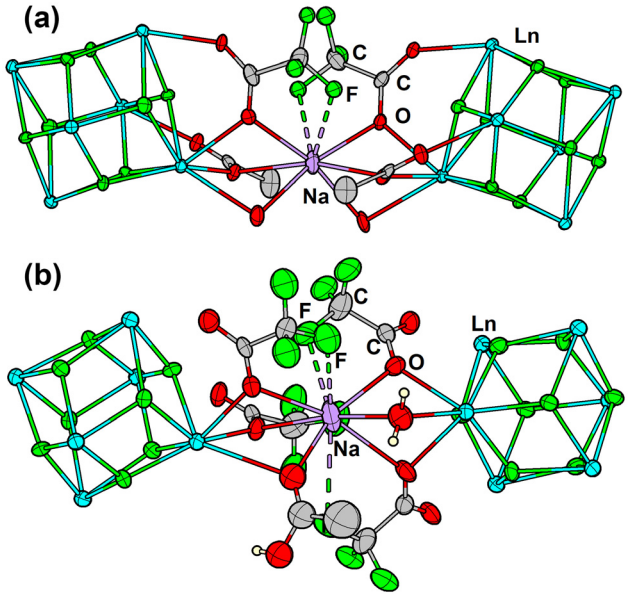

Fig. 5 Binding sodium atom between two $\{Ln_6F_8\}$ fragments in **IIb** (a) and **III** (b) structures (short Na–F contacts are shown in dashed lines).

sodium atom surrounding decreases for heavier lanthanides, which confirms the above trend (Fig. S17).

The sodium ions are linked to the anion complexes in the same way as realized in the fluorotrifluoroacetate of 3d-metals.[22] Fluorotrifluoroacetate families containing 4f- and 3d-elements are similar, with the difference in their crystal structures determined by atom radii, resulting in differences in preferred coordination numbers. Based on the structure data for recently published fluorotrifluoroacetate complexes with 3d-metals,[4,23] it was concluded that varying the cations in the lanthanide family of complexes also allows us to obtain substances with various packing of the anion complex and different structure dimensions.

In the next section, the structural features of **I–VI**, which have different axial ligand sets and packing, will be considered.

3.1.1. Structural features of compounds I, IV, V. Three of the obtained compounds are isostructural (**I**, **IV**, **V**) and crystallize in the $P\bar{1}$ space group. Here, we describe the structure of these compounds with the example of compound **IV** ($Na_2[Dy_6(\mu_3\text{-}F_8)(tfa)_{12}(Htfa)_2(H_2O)_4](Htfa)_{0.5}$). There are six independent dysprosium atoms in the structure of **IV**. Dy1–Dy3 and Dy4–Dy6 belong to two neighboring anion complexes $[Dy_6(\mu_3\text{-}F_8)(tfa)_{12}(H_2O)_4(Htfa)_2]^{2-}$ (Fig. 6). Axial ligand positions are occupied by oxygen atoms of trifluoroacetic acid (Dy1, Dy6) or water (Dy2–Dy5) molecules. One solvate molecule of trifluoroacetic acid is also present in the structure; it forms one hydrogen bond O34–H34A···O43 with the oxygen atom of the water molecule coordinated by Dy5 (Fig. 7).

The triclinic compound **IV** contains two crystallographically independent sodium atoms (Na1 and Na2). Each anion complex is connected with four sodium atoms; thus, layers in the structure of **IV** are formed (Fig. 8). The layers are arranged parallel to the $\{bc\}$ plane. Molecules of solvate acid are observed between the layers but do not connect them.

3.1.2. Structural features of compounds IIa and III. Compounds $Na_2[Eu_6(\mu_3\text{-}F_8)(tfa)_{12}(H_2O)_{5.12}(Htfa)_{0.88}]$ (**IIa**) and $Na_2[Tb_6(\mu_3\text{-}F_8)(tfa)_{12}(H_2O)_{5.12}(Htfa)_{0.88}]$ (**III**) crystallize in $P2_1/n$ and are isostructural. Here, we describe the structure of this pair of substances using **IIa** as an example.

There are three crystallographically independent lanthanide atoms in the structure of **IIa**. These three lanthanide atoms, along with their symmetry equivalents, form one hexanuclear anion complex $[Eu_6(\mu_3\text{-}F_8)(tfa)_{12}(H_2O)_{5.12}(Htfa)_{0.88}]^{2-}$. An axial position on Eu1 atom is occupied by an oxygen atom from statistically disordered molecules of trifluoroacetic acid, O13, or

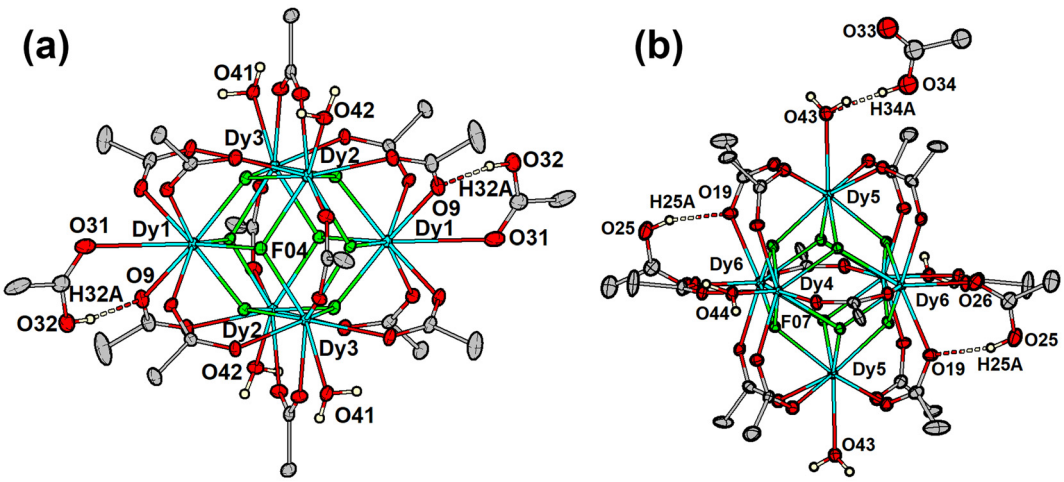

Fig. 6 Crystal structure of the anion complex $[Dy_6(\mu_3\text{-}F_8)(tfa)_{12}(H_2O)_4(Htfa)_2]^{2-}$ in **IV** (a) and its bond with solvate Htfa molecule (b). Fluorine atoms of the CF_3-groups are omitted for clarity.

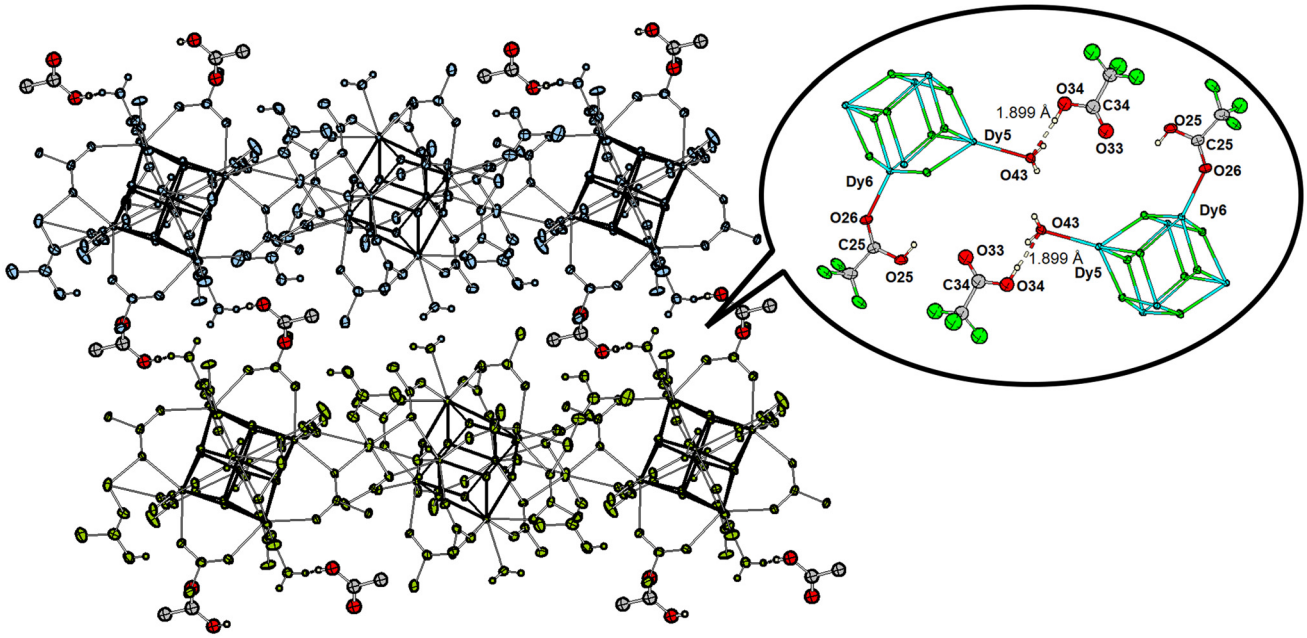

Fig. 7 Solvate trifluoroacetic acid molecule between two neighboring layers (shown in different colors). Fluorine atoms of the CF_3-groups are omitted for clarity.

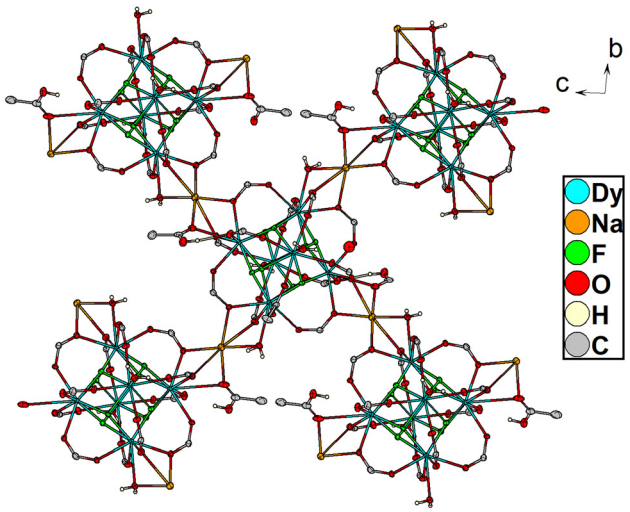

Fig. 8 Cationic–anionic layer in the crystal structure of **IV**, viewed along the crystallographic axis *a*. Fluorine atoms of the CF_3-groups are omitted for clarity.

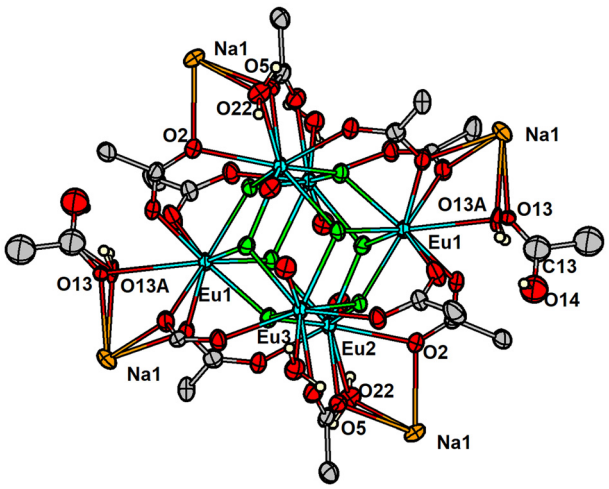

Fig. 9 Structure of the anion complex $[Eu_6(\mu_3\text{-}F_8)(tfa)_{12}(H_2O)_{5.12}(Htfa)_{0.88}]^{2-}$ of **IIa** with the nearest sodium cations. The statistical disorder of axial ligands coordinated by Eu1 atoms is shown. Fluorine atoms of the CF_3-groups are omitted for clarity.

water, O13A (with occupancy 0.44 and 0.56, respectively, according to SCXRD refinement data), as shown in Fig. 9.

The water molecules' oxygen atoms O22 and O21 complete the coordination environment of the Eu2 and Eu3 atoms, respectively. The O22 atom is also linked to the sodium atom Na1 and plays a bridging role.

In contrast to the triclinic phases described above, **IIa** has a single independent sodium atom. However, the same kinds of cation–anionic layers are observed, which are parallel to the {*bc*} plane, as in the triclinic compounds (Fig. 10).

3.1.3. Structural features of compound IIb. Crystals of another compound obtained in the europium system have higher symmetry (space group $R\bar{3}$) and the composition $Na_{1.5}(H_3O)_{0.5}[Eu_6(\mu_3\text{-}F_8)(tfa)_{12}(Htfa)_{0.5}(H_2O)_{5.5}](Htfa)_{0.5}$. The structure contains four crystallographically independent europium atoms that form two anionic complexes (Fig. 11). The six crystallographically equivalent Eu4 atoms form the first anion $[Eu_6(\mu_3\text{-}F_8)(tfa)_{12}(H_2O)_6]^{2-}$, while Eu1–Eu3 form another anion, $[Eu_6(\mu_3\text{-}F_8)(tfa)_{12}(Htfa)_{0.96}(H_2O)_{5.04}]^{2-}$. The coordination sphere of Eu1 includes different statistically disordered ligands in the

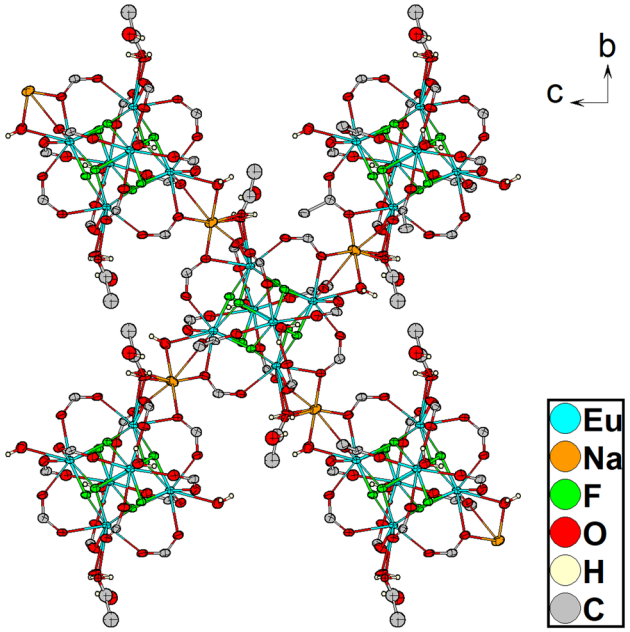

Fig. 10 Cationic-anionic layers in the crystal structure of **IIa**, viewed along the crystallographic axis *a*. Fluorine atoms of the CF_3-groups are omitted for clarity.

axial position, a water molecule with donor atom O21, and a molecule of trifluoroacetic acid connected to Eu1 by its carbonyl oxygen atom O17A. The water molecule mentioned above also takes part in hydrogen bond formation with the solvate trifluoroacetic acid molecule that has the same chemical occupancy.

The single independent sodium atom in the structure of **IIb** is linked to the anion complexes. Furthermore, anions formed by Eu4 atoms have six neighboring $\{Ln_6(\mu_3\text{-}F)_8\}$ fragments, and those formed by Eu1–Eu3 atoms have only two neighboring fragments (Fig. 12). Thus, **IIb** exhibits a net-like organization.

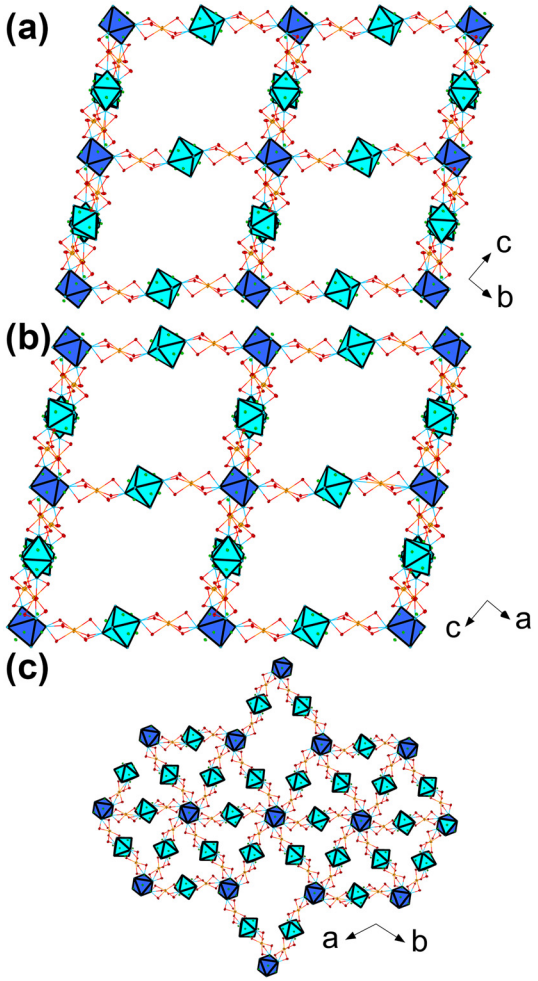

Fig. 12 Projection of frameworks (only $\{Ln_6\}$ fragments and Na ions with binding oxygen atoms are shown) along the *a*, *b*, and *c* axes, respectively (a–c) in the **IIb** structure. Symmetrically independent $\{Ln_6\}$ units are presented in different colours: blue octahedra correspond to $\{Ln_6\}$ units of Eu4 atoms and turquoise octahedra correspond to $\{Ln_6\}$ units consisting of Eu1–Eu3 atoms.

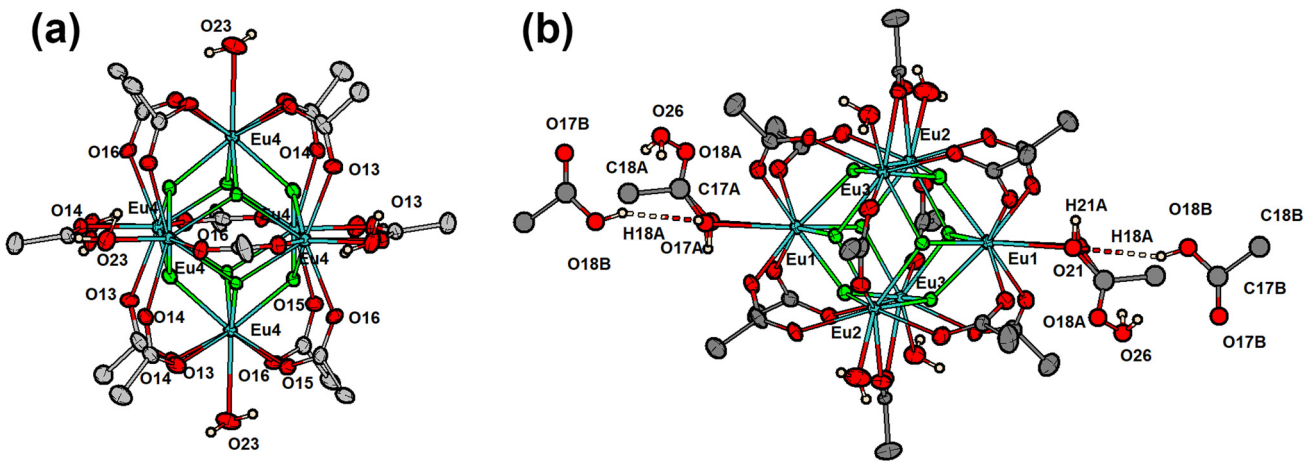

Fig. 11 Two types ((a) and (b)) of anionic complexes in the crystal structure of **IIb**. The statistical disorder of axial ligands coordinated by Eu1 atom and hydrogen bonds is shown. Fluorine atoms of the CF_3-groups are omitted for clarity.

The sodium cations in **IIb** cannot compensate for the anion charges completely, so the electroneutrality principle requires the presence of another counterion. The only such counterion may be the hydroxonium cation located in the cavities of the cation–anionic framework (Fig. 13). Apparently, there are two independent H_3O^+ ions connected to disordered water molecules (O27–O30). The localization of the hydrogen atoms in these H_2O molecules looks impossible based on the available data.

3.1.4. Structural features of compounds VI. The potassium compound $K_2[Yb_6(\mu_3\text{-}F)_8(tfa)_{12}(H_2O)_5](Htfa)_2(H_2O)$ crystallizes in a triclinic crystal system (space group $P\bar{1}$) and has three crystallographically independent ytterbium atoms that form the anion complex $[Yb_6(\mu_3\text{-}F_8)(tfa)_{12}(H_2O)_5]^{2-}$. Neighboring ytterbium atoms are connected by bridging bidentate trifluoroacetate anions, one of which (O11A–C11A(C12A)–O12A) is disordered; it partially connects the Yb2 and Yb3 atoms and partially Yb2 and K1. In the latter case, the position of the carboxylic atom O11A is occupied by atom O22B of the water molecule (Fig. 14). The coordination environment of Yb3 (CN = 9) contains four fluorine atoms, three oxygen atoms from bridging trifluoroacetate anions (O3, O5, O10), one oxygen atom from a water molecule and disordered atoms O11A and O22B (from a tfa ion or water molecule). In case of the Yb2 atom (CN = 8), the coordination environment is formed by four fluorine atoms, three oxygen atoms of bridging trifluoroacetate anions (O1, O6, O7), and an oxygen atom (O12A or O12B) of a disordered trifluoroacetate anion that links Yb2 with Yb3 or K1. The atoms in the coordination environment of Yb1 (CN = 9) are common to the above and the axial position is occupied by a water molecule (O23).

Each anion complex is surrounded by four potassium atoms. The environment of the cation contains four oxygen atoms of bidentate trifluoroacetate anions, the disordered

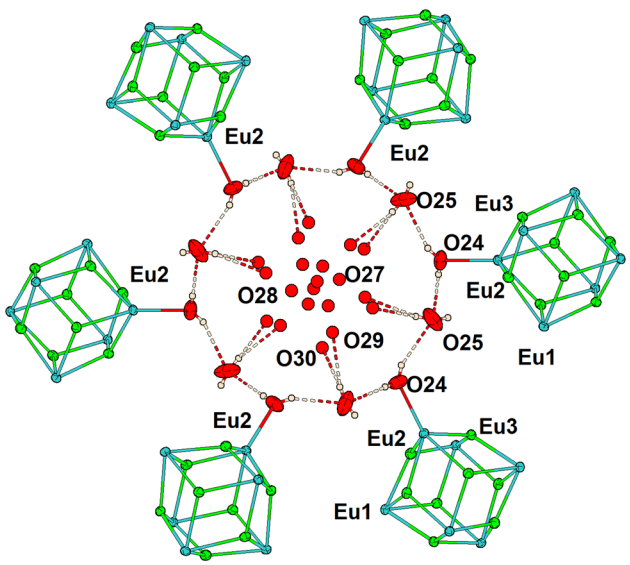

Fig. 13 Void in the structure of **IIb** filled by H_3O^+ cations and solvate water molecules.

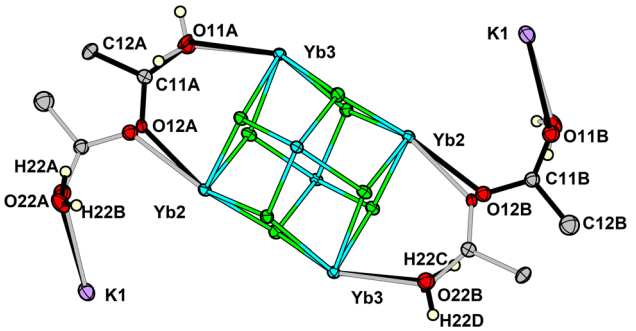

Fig. 14 Structure of the anionic $[Yb_6(\mu_3\text{-}F)_8(tfa)_{12}(H_2O)_5]^{2-}$ complex in **VI** with the nearest potassium cations. The statistical disorder of ligands coordinated by Yb2 and Yb3 atoms is shown. Two bond colours (black and gray) correspond to A and B parts of the disordered structure. Fluorine atoms of the CF_3-groups are omitted for clarity.

oxygen atoms O11B and O22A (see above), and the carbonyl oxygen atom O14 of the trifluoroacetic acid. The hydroxy group of this acid (O13A–H13A) forms a hydrogen bond with partially occupied atoms O11B and O22A (d(O···O) is 2.767(9) and 2.558 (7) Å, respectively). The anion complexes are linked *via* potassium atoms into infinite chains placed along the crystallographic axis b (Fig. 15). Distances between neighboring chains (or layers in cases compounds **I–V**) correspond to van der Waals interactions between fluorine atoms of trifluoroacetate groups belonging to adjacent chains (layers).

3.1.5. General crystallochemical comments. Three types of lanthanide atoms can be distinguished in the structures of **I–VI**. The first type of atom ("Ln_{Htfa}") has an oxygen atom of trifluoroacetic acid in the axial position. The same oxygen atom (excluding those in the structure of **IIb**) also enters the environment of the alkali metal atom. The second atom type ("Ln_{H_2ONa}") has a water oxygen atom in the axial position. Additionally, this oxygen atom is connected to an alkali metal atom. The third atom type ("Ln_{H_2O}") has a terminal water molecule in the axial position.

Ln–F and Ln–O distances are almost the same for each lanthanide atom within each structural function. A full set of this distance data is given in Table S5; Table 2 contains the average distances for each lanthanide atom type.

According to the data, Ln–F distances increase in the series Ln_{Htfa}–F, Ln_{H_2ONa}–F, and Ln_{H_2O}–F. A slight increase of the "Ln_{Htfa}"–O_{tfa} distance (O_{tfa} is an oxygen atom of the bridging trifluoroacetate anion) is caused by participation of this oxygen atom in intramolecular hydrogen bonds. In contrast to Ln–F distances, the bond length of Ln–O for the axial oxygen atom reduces in the series Ln_{Htfa}–F, Ln_{H_2ONa}–F, and Ln_{H_2O}–F.

The currently available structural data for the $[Ln_6(\mu_3\text{-}F_8)(RCOO)_{12}]$ fragment are summarized in Table 3. It lists the average Ln–Ln, Ln–F and Ln–O distances for the compounds obtained in this work, as well as for previously reported compounds.

As shown in Table 3, a lanthanide coordination number of nine is observed in most of the compounds. However, there

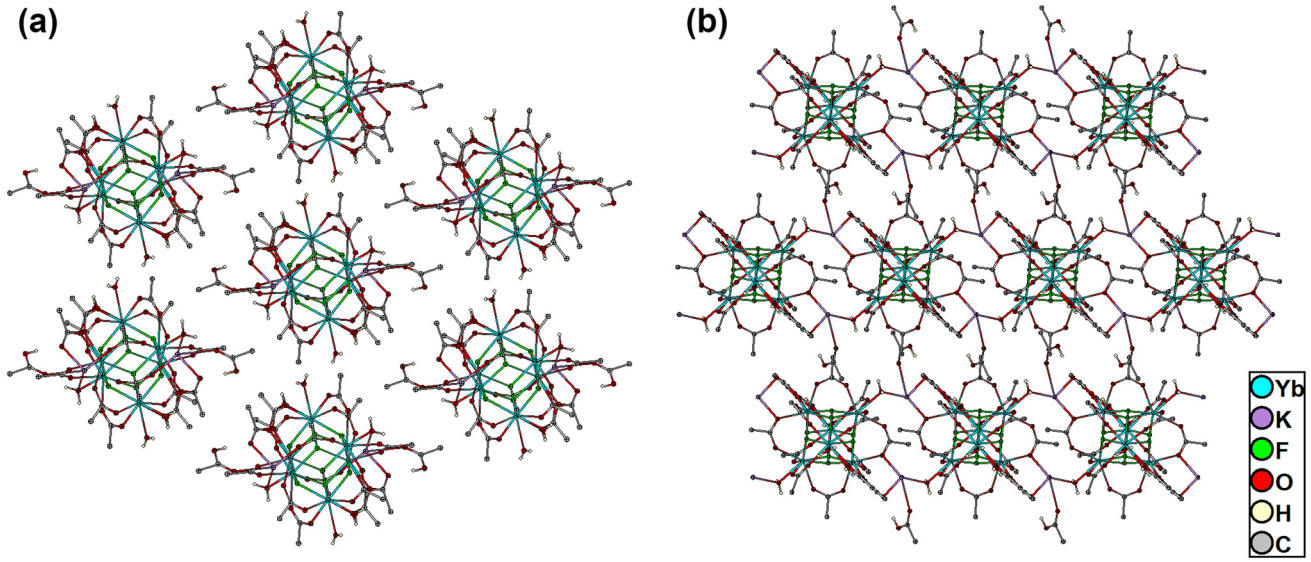

Fig. 15 Polymeric chains in the structure of **VI** perpendicular to (a) and along (b) the *b* crystallographic axis. Fluorine atoms of the CF_3-groups are omitted for clarity.

Table 2 Average Ln–F and Ln–O distances in structures **I–VI**. Lanthanide atoms are grouped according to their type

	I	IIa	IIb	III	IV	V	VI
Ln_{Htfa}–F	2.414(3)	2.361(4)	2.383(4)	2.334(6)	2.321(3)	2.276(3)	2.247(2)
$Ln_{H_2ONa/K}$–F	2.416(3)	2.370(4)	2.368(4)	2.337(6)	2.335(3)	2.307(3)	2.326(2)
Ln_{H_2O}–F	2.454(3)	2.402(4)	2.378(4)	2.384(6)	2.370(3)	2.343(3)	2.340(2)
Ln_{Htfa}–O_{tfa}	2.488(4)	2.414(6)	2.390(5)	2.386(8)	2.363(4)	2.320(3)	2.291(5)
$Ln_{H_2ONa/K}$–O_{tfa}	2.476(4)	2.408(6)	2.409(5)	2.379(8)	2.364(3)	2.321(3)	2.307(3)
Ln_{H_2O}–O_{tfa}	2.459(4)	2.394(6)	2.402(5)	2.359(8)	2.351(4)	2.314(3)	2.322(7)
Ln_{Htfa}–O_{Htfa}	2.750(4)	2.879(19)	2.662(19)	3.02(3)	2.974(5)	3.252(5)	—
$Ln_{H_2ONa/K}$–O_{H_2O}	2.671(4)	2.623(11)	2.633(6)	2.70(2)	2.609(4)	2.613(3)	
Ln_{H_2O}–O_{H_2O}	2.573(4)	2.524(6)	2.575(13)	2.515(8)	2.508(4)	2.488(4)	

Table 3 Summarized average distances in the previously reported compounds containing the$[Ln_6(\mu_3\text{-}F_8)(RCOO)_n]$ fragment, where R = CF_3 (tfa), C_2F_5 (pfa), $(CH_3)_3C$ (piv), or C_6H_4COO (dbc) and *n* = 10 or 12. Green, gold and blue-coloured rows correspond to the structures with 9-, 8- and mixed (8 and 9)-coordinated lanthanide atoms, respectively

			Ln–O average						
Ln	Ln···Ln average	Ln–F average	O_{tfa}	O_{pfa}	O_{piv}	O_{dbc}	$Ln–O_L$ average	*T* measurement, K	Ref.
Pr	**4.0738(5)**	**2.428(3)**	**2.474(4)**				**2.665(4)**	**150(2)**	**This work (I)**
Eu	**3.9859(7)**	**2.378(4)**	**2.405(6)**				**2.632(12)**	**150(2)**	**This work (IIa)**
	3.9804(9)	**2.376(4)**	**2.400(5)**				**2.58(1)**	**100(2)**	**This work (IIb)**
	4.005(2)	2.386(13)	2.403(18)				2.670(19)	223(2)	10
	3.9787(8)	2.373(3)		2.396(4)			2.663(4)	120(2)	10
Tb	**3.9457(8)**	**2.352(6)**	**2.375(8)**				**2.683(16)**	**150(2)**	**This work (III)**
	3.9687(17)	2.384(10)			2.349(12)		2.389(18)	298(2)	9
	3.9161(12)	*2.344(2)*				*2.338(6)*	—	*150(2)*	8
Dy	**3.9232(6)**	**2.342(3)**	**2.359(4)**				**2.697(5)**	**100(2)**	**This work (IV)**
Ho	*3.8613(9)*	*2.312(2)*				*2.306(4)*	—	*105(2)*	7
Tm	**3.8617(5)**	**2.309(3)**	**2.318(3)**				**2.551(4)**	**100(2)**	**This work (V)**
Yb	**3.8537(4)**	**2.304(2)**	**2.307(5)**				**2.445(6)**	**100(2)**	**This work (VI)**
	3.8340(6)	2.294(2)	2.304(3)				2.496(2)	120(2)	6

are some examples in which the coordination is reduced to eight due to the small lanthanide radius (Yb compounds) and bulky sterically hindered carboxylate anions (piv or bdc). The presence of an available axial site in most cases can be used to place antenna ligands that can enhance the luminescence of such compounds.

The $\{Ln_6(\mu_3\text{-}F)_8\}$ rhombododecahedral sizes vary over a wide range. This may indicate that such the units with can apparently be formed for the most lanthanides. This fact makes it possible to obtain heterometallic compounds based on this core.

3.2. Thermal properties

The thermal properties of compounds were investigated in an Ar atmosphere with compounds **IIb**, **III**, **IV** and **VI** selected as representatives of each structural type. Their decomposition leads to a mixture of complexes of fluoride $MLnF_4$ (M = Na, K; $Na_5Eu_9F_{32}$ in case **IIb**) and lanthanide fluoride LnF_3 (Fig. S21–S24) according to the PXRD data for the solid residues. In all cases, decomposition was staggered. The first stage was characterized by the separation of solvate molecules if they are present in the compound (temperature 100–150 °C, observed for **IIb** and **IV**) or crystallization water molecules (temperature 150–200 °C). During the next decomposition stage, anion complexes in every compound are destroyed. The decomposition temperature depends on the cation and is in the range 250–300 °C for **IIb**, **III**, and **IV**, which includes sodium cations, while the potassium compound **VI** completes decomposition at lower temperatures (220–250 °C).

Gas products of decomposition were determined to be in the *m*/*z* range 16–70 using a mass analyzer. As expected, the ion currents for particles that are characteristic for trifluoroacetic acid[24] and water had considerable intensity (44 (CO_2), 69 (CF_3), 16 (O), 17 (OH), and 18 (H_2O)). In the first stage, species with *m*/*z* 16, 17, 18 are observed for all compounds, which correspond to the removal of solvate water molecules. For compound **IV**, the removal of one solvate trifluoroacetic acid molecule was also observed. Simultaneously, weak peaks appear in the ion current curves at *m*/*z* 44 and 69. The assumed elimination of H_2O and Htfa molecules was confirmed by weight loss calculations.

No distinct first stage of decomposition was observed for compound **IIb**, owing to the large amount of solvate water molecules linked together in the complex hydrogen bonding system. Its dehydration takes place smoothly in a temperature range of 100–200 °C.

The main mass losses are observed in the second stage of the decomposition over a narrow temperature interval. The heat release effect observed during this stage, according to the DSC curve, may indicate a mass removal effect. Such phenomena lead to slight differences between the calculated and experimental mass loss. An absence of pyrohydrolysis may be confirmed by the absence of peaks for the oxide/oxofluoride phases in the PXRD patterns of the decomposition products.

3.3. Luminescence properties

Given that the $\{Ln_6(\mu_3\text{-}F)_8\}$ core exhibits features that constitute an attractive "building block" for obtaining efficient photoluminescent materials, the spectroscopic properties of the europium, terbium and dysprosium complexes were studied in detail.

In contrast to the luminescent complexes of lanthanides with aromatic[25] and heteroaromatic carboxylic acids[1] and acylpyrazolones,[26] the excitation spectra of complexes **IIb**, **III** and **IV** (Fig. S25) do not contain π–π bands of the ligand but contain pronounced electronic transitions of lanthanides. This is certainly because the intrinsic absorption of trifluoroacetate ligands is in the hard UV range (λ < 250 nm). Nevertheless, compounds **IIb** and **III** under UV irradiation exhibit intense red and green luminescence, respectively, visible to the naked eye. The yellow-green luminescence of the **IV** complex is much less bright.

The luminescence spectrum of Eu contains bands related to europium transitions $^5D_0 \rightarrow {}^7F_j$, j = 0–4.[27] Interestingly, transitions from higher $^5D_1$ and $^5D_2$ levels do not appear, although they can often be observed for such rigid high-symmetry systems.[27,28] The hypersensitive transition $^5D_0$–$^7F_2$ is the most intense.

The splitting of the least intense $^5D_0 \rightarrow {}^7F_0$ transition is well described by a single Gaussian curve, peaking at 17 254 cm^{-1} (579.6 nm) (Fig. S26). This transition cannot split in any symmetry field, making it a marker for nonequivalent europium cations in the structure.[28] The lack of splitting indicates a high symmetry in the coordination environment of Eu1–Eu4 atoms. Analysis using the SHAPE 2.1 program[19,29] suggests that this environment is best represented as a one-capped square antiprism (C_{4v}) or a Muffin (C_s), with the former being more accurate. For these symmetries, the $^5D_0 \rightarrow {}^7F_1$ transition should split into 2 or 3 components,[28,30] but the observed spectrum shows four components, three of which are dominant and one weak. This suggests that the "extra" components of the $^5D_0 \rightarrow {}^7F_1$ transition are linked to nonequivalent europium cations, especially given the small energy differences between them (Fig. S27). The hypersensitive $^5D_0 \rightarrow {}^7F_2$ transition is the most intense, with four components identified (Fig. S28), consistent with predictions from Judd–Ofelt theory for C_{4v} symmetry.[28]

Integration of the spectrum components (Table S13) allows us to calculate the radiative τ_{rad} of europium ions, which is 4370 μs. Luminescence decay curves of the Eu complex at 77 K and at room temperature are described by the monoexponential law, $I = I_0 e^{-\frac{t}{\tau_{obs}}}$. The values of τ_{obs} at 300 K and 77 K are (981.3 ± 0.4) μs (Fig. S29) and (1002.0 ± 0.4) μs (Fig. S30), respectively. Thus, the temperature dependence of τ_{obs} is small, which correlates well with the rigid crystal structure of **IIb** and the absence of vibrational quenching on OH, CH, or NH bonds, which is common for most europium[27] complexes. The internal quantum yield, $\Phi_{Ln}^{Ln} = \frac{\tau_{obs}}{\tau_{rad}}$, is 22.5 and 22.9% at 300 K and 77 K, respectively.

The luminescence spectra of **III** and **IV** (Fig. 16), as well as in the case of the europium complex considered above, do not contain any bands, except for the transitions of these ions from the most stable excited terms $^5D_4$ (Tb) and $^7F_{9/2}$ (Dy)

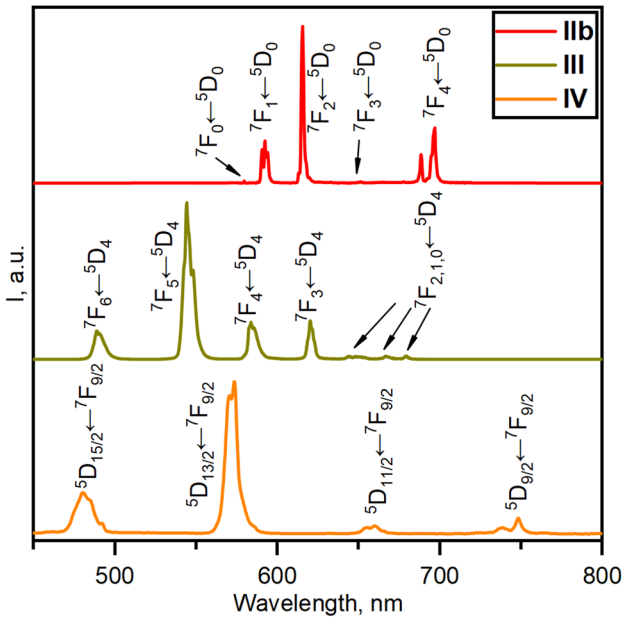

Fig. 16 High-resolution emission spectra of **IIb**, **III**, and **IV** recorded at 77 K (λ_{ex} = 395, 385 and 393 nm, respectively).

to the sublevels of the main multiplet ^7F_j, j = 6–0 (Tb) and ^5D_j, j = 15/2–9/2 (Dy). The most intense transition of terbium ions (j = 5) has a maximum at 545 nm, which corresponds to bright green luminescence. It is interesting that transitions with j = 2,1 and 0, which usually do not appear in organic complexes, but are often found in solid-state phosphors,[27] appear as low-intensity bands in the red region of the spectrum. The most intense Dy transition (j = 13/2) has a maximum at 575 nm, providing yellow-green luminescence of the Dy complex. The observed lifetimes of terbium and dysprosium complexes are (2563.4 ± 0.8) μs (Fig. S31) and (34.4 ± 0.4) μs (Fig. S32), respectively. In both the cases, one can speak of very high values of τ_{obs}, exceeding most of the carboxylate complexes, which is associated with the suppression of vibrational quenching in the rigid fluoroacetate framework.[1]

4. Conclusion

The hexanuclear fluorocarboxylate anion $[Ln_6(\mu_3\text{-}F)_8(tfa)_{12}L_6]^{2-}$ that is present in **I–VI** and in some compounds described earlier[6,10] appears to be a common stable structural core for the whole class of rare-earth fluorocarboxylate complexes. Herein, we report a simple synthesis of seven new fluorine-rich compounds containing the $\{Ln_6(\mu_3\text{-}F)_8\}$ core. The growth of crystals of the target substances confirms the good yields and reproducibility of the synthesis of **I–VI**, although their rich crystallochemistry (three different sodium phases with slight differences in composition and structure) and associated phase interconversions require further study. Nevertheless, the results obtained allow us to reach a number of conclusions regarding the stability of the $\{Ln_6(\mu_3\text{-}F)_8\}$ fragment for a wide range of rare-earth ions (Pr–Yb) despite the noticeable effect of the lanthanide contraction.

Investigations on the luminescence properties of **IIb**, **III** and **IV** revealed the high lifetime of the excited state, along with weak dependence of the photophysical characteristics on temperature, which may be explained by the rigid nature of the central fluorinated fragment containing the lanthanide ions. The six close crystallographic metal positions in the core open great opportunities for the syntheses of bimetallic systems. For example this can allow to reach decreasing of the concentration quenching and to obtain systems with sensibilisation or up-conversion effects.

The family of compounds is a good base for creating new luminescent materials due to its thermal stability and wide range of rare earth elements which can form this structures.

Conflicts of interest

There are no conflicts to declare.

Data availability

The data supporting this article have been included as part of the SI.

Supplementary information (synthesis details, X-ray diffraction data, IR spectra, selected crystallographic data, decomposition details and luminescence spectra) is available. See DOI: **https://doi.org/10.1039/d5dt01105a**

CCDC 2391137–2391142 and 2427723 contain the supplementary crystallographic data for this paper.[31a–g]

Acknowledgements

The study was conducted under the state assignment of Lomonosov Moscow State University, project no. AAAA-A21-121011590082-2.

This research was carried out with partial support from MSU Shared Research Equipment Center “Technologies for obtaining new nanostructured materials and their complex study”, National Project “Science” and MSU Program of Development.

This research was partially performed using the equipment of the JRC PMR IGIC RAS.

References

1 Y. A. Belousov, A. A. Drozdov, I. V. Taydakov, F. Marchetti, R. Pettinari and C. Pettinari, *Coord. Chem. Rev.*, 2021, **445**, 214084.
2 Y. Hasegawa and T. Nakanishi, *RSC Adv.*, 2015, **5**, 338–353.
3 M. L. Aulsebrook, B. Graham, M. R. Grace and K. L. Tuck, *Coord. Chem. Rev.*, 2018, **375**, 191–220.
4 M. E. Buzoverov, T. Y. Glazunova, V. E. Gontcharenko and I. V. Morozov, *Z. Kristallogr. – Cryst. Mater.*, 2023, **238**, 363–371.

5 M. E. Buzoverov, T. Y. Glazunova and E. K. Lermontova, *Mendeleev Commun.*, 2022, **32**, 212–214.
6 F. Morsbach and W. Frank, *Acta Crystallogr., Sect. E: Crystallogr. Commun.*, 2022, **78**, 608–614.
7 J. P. Vizuet, M. L. Mortensen, A. L. Lewis, M. A. Wunch, H. R. Firouzi, G. T. McCandless and K. J. Balkus, *J. Am. Chem. Soc.*, 2021, **143**, 17995–18000.
8 Z. Ajoyan, G. A. Mandl, P. R. Donnarumma, V. Quezada-Novoa, H. A. Bicalho, H. M. Titi, J. A. Capobianco and A. J. Howarth, *ACS Mater. Lett.*, 2022, **4**, 1025–1031.
9 B.-K. Ling, J. Li, Y.-Q. Zhai, H.-K. Hsu, Y.-T. Chan, W.-P. Chen, T. Han and Y.-Z. Zheng, *Chem. Commun.*, 2020, **56**, 9130–9133.
10 F. Morsbach, S. Klenner, R. Pöttgen and W. Frank, *Dalton Trans.*, 2022, **51**, 4814–4828.
11 V. Petříček, L. Palatinus, J. Plášil and M. Dušek, *Z. Kristallogr. – Cryst. Mater.*, 2023, **238**, 271–282.
12 *SMART (control) and SAINT (integration) software, version 5.0*, Bruker AXS Inc., Madison, WI, 1997.
13 G. M. Sheldrick, *SADABS. Program for scaling and correction of area detector data*, University of Göttingen, Germany, 1997.
14 G. M. Sheldrick, *Acta Crystallogr., Sect. A:Found. Crystallogr.*, 2008, **64**, 112–122.
15 V. S. Oliveira, D. M. A. Melo, Z. Rocha da Silva, L. Zinner and K. Zinner, *J. Alloys Compd.*, 2000, **303–304**, 157–161.
16 J. She, D. Li, C. Hou, W. Yang, W. Wei and B. Peng, *J. Rare Earths*, 2011, **29**, 193–197.
17 T. J. Boyle, D. T. Yonemoto, J. M. Sears, L. J. Treadwell, N. S. Bell, R. E. Cramer, M. L. Neville, G. A. K. Stillman and S. P. Bingham, *Polyhedron*, 2017, **131**, 59–73.
18 Z. Ajoyan, G. A. Mandl, P. R. Donnarumma, V. Quezada-Novoa, H. A. Bicalho, H. M. Titi, J. A. Capobianco and A. J. Howarth, *ACS Mater. Lett.*, 2022, **4**, 1025–1031.
19 M. Llunell, D. Casanova, J. Cirera, P. Alemany and S. Alvarez, Users Manual: SHAPE. Program for the Stereochemical Analysis of Molecular Fragments by Means of Continuous Shape Measures and Associated Tools, 2013, pp. 1–35.
20 R. D. Shannon, *Acta Crystallogr., Sect. A*, 1976, **32**, 751–767.
21 V. A. Blatov and V. N. Serezhkin, *Crystallogr. Rep.*, 1995, **40**, 302–307.
22 I. V. Morozov, E. V. Karpova, T. Yu. Glazunova, A. I. Boltalin, M. A. Zakharov, D. S. Tereshchenko, A. A. Fedorova and S. I. Troyanov, *Koord. Khim.*, 2016, **42**, 609–623.
23 D. S. Tereshchenko, I. V. Morozov, A. I. Boltalin, E. V. Karpova, T. Y. Glazunova and S. I. Troyanov, *Crystallogr. Rep.*, 2013, **58**, 68–77.
24 NIST Mass Spectrometry Data Center and W. E. Wallace, Mass Spectra, in *NIST Chemistry WebBook*, NIST Standard Reference Database Number 69, ed. P. J. Linstrom and W. G. Mallard, National Institute of Standards and Technology, Gaithersburg MD, 2025, p. 20899, DOI: **10.18434/T4D303**, (retrieved March 13, 2025).
25 R. Janicki, A. Mondry and P. Starynowicz, *Coord. Chem. Rev.*, 2017, **340**, 98–133.
26 F. Marchetti, R. Pettinari and C. Pettinari, *Coord. Chem. Rev.*, 2015, **303**, 1–31.
27 J.-C. G. Bünzli and S. V. Eliseeva, in *Lanthanide Luminescence. Springer Series on Fluorescence*, Springer, Berlin, Heidelberg, 2010, vol. 7, pp. 1–45.
28 K. Binnemans, *Coord. Chem. Rev.*, 2015, **295**, 1–45.
29 A. Ruiz-Martínez, D. Casanova and S. Alvarez, *Dalton Trans.*, 2008, 2583–2591.
30 G. Vicentini, L. B. Zinner, J. Zukerman-Schpector and K. Zinner, *Coord. Chem. Rev.*, 2000, **196**, 353–382.
31 (*a*) E. D. Boltkov, M. E. Buzoverov, E. Kh. Lermontova, Yu. A. Belousov, D. A. Steshenko, V. E. Gontcharenko and T. Yu. Glazunova, 2025, CCDC 2391137: Experimental Crystal Structure Determination, DOI: **10.5517/ccdc.csd.cc2l85gj**; (*b*) E. D. Boltkov, M. E. Buzoverov, E. Kh. Lermontova, Yu. A. Belousov, D. A. Steshenko, V. E. Gontcharenko and T. Yu. Glazunova, 2025, CCDC 2391138: Experimental Crystal Structure Determination, DOI: **10.5517/ccdc.csd.cc2l85hk**; (*c*) E. D. Boltkov, M. E. Buzoverov, E. Kh. Lermontova, Yu. A. Belousov, D. A. Steshenko, V. E. Gontcharenko and T. Yu. Glazunova, 2025, CCDC 2391139: Experimental Crystal Structure Determination, DOI: **10.5517/ccdc.csd.cc2l85jl**; (*d*) E. D. Boltkov, M. E. Buzoverov, E. Kh. Lermontova, Yu. A. Belousov, D. A. Steshenko, V. E. Gontcharenko and T. Yu. Glazunova, 2025, CCDC 2391140: Experimental Crystal Structure Determination, DOI: **10.5517/ccdc.csd.cc2l85km**; (*e*) E. D. Boltkov, M. E. Buzoverov, E. Kh. Lermontova, Yu. A. Belousov, D. A. Steshenko, V. E. Gontcharenko and T. Yu. Glazunova, 2025, CCDC 2391141: Experimental Crystal Structure Determination, DOI: **10.5517/ccdc.csd.cc2l85ln**; (*f*) E. D. Boltkov, M. E. Buzoverov, E. Kh. Lermontova, Yu. A. Belousov, D. A. Steshenko, V. E. Gontcharenko and T. Yu. Glazunova, 2025, CCDC 2391142: Experimental Crystal Structure Determination, DOI: **10.5517/ccdc.csd.cc2l85mp**; (*g*) E. D. Boltkov, M. E. Buzoverov, E. Kh. Lermontova, Yu. A. Belousov, D. A. Steshenko, V. E. Gontcharenko and T. Yu. Glazunova, 2025, CCDC 2427723: Experimental Crystal Structure Determination, DOI: **10.5517/ccdc.csd.cc2mh7n1**.